

Theory of multiple magnetic scattering for quasiparticles on a gapless topological insulator surface

Zhen-Guo Fu,^{1,2} Ping Zhang,^{2,*} Zhigang Wang,² Fawei Zheng,² and Shu-Shen Li^{1,†}

¹*SKLSM, Institute of Semiconductors, CAS,
P. O. Box 912, Beijing 100083, China*

²*LCP, Institute of Applied Physics and Computational Mathematics,
P.O. Box 8009, Beijing 100088, China*

Abstract

We develop a general low-energy multiple-scattering partial-wave theory for gapless topological insulator (TI) surfaces in the presence of magnetic impurities. As applications, we discuss the differential cross section (CS) $d\Lambda/d\varphi$, the total CS Λ_{tot} , the Hall component of resistivity Ω , and inverse momentum relaxation time Γ_M for single- and two-centered magnetic scattering. We show that differing from the nonmagnetic impurity scattering, s -wave approximation is not advisable and convergent in the present case. The symmetry of CS is reduced and the backscattering occurs and becomes stronger with increasing the effective magnetic moment M of single magnetic impurity. We show a non-zero perpendicular resistivity component Ω , which may be useful for tuning the Hall voltage of the sample. Consistent with the analysis of $d\Lambda/d\varphi$, by comparing Γ_M with Λ_{tot} , we can determine different weights of backscattering and forward scattering. Similar to CS, Ω and Γ_M also exhibit oscillating behavior for multiple magnetic scattering centers due to interference effect.

PACS numbers: 72.10.-d, 72.10.Fk, 73.20.-r, 73.50.Bk

*zhang_ping@iapcm.ac.cn

†sslee@semi.ac.cn

I. INTRODUCTION

A topic of fundamental importance in condensed matter physics is how the presence of defects or impurities induce strong modifications on the local electronic properties of crystalline solids. These modifications, with the stunning development of scanning tunneling microscopy (STM), have been extensively investigated on metal surfaces where they are well known as Friedel oscillations and manifest as standing waves in the local electronic density spanning regions up to ~ 10 nm from the defects on the metal surfaces. One kind of particularly suitable prototype that have been used in a large amount of STM measurements to study the effects of impurity and the formation of adsorbate superstructure are the (111) surfaces of noble metals, on which the surface-state electrons form a two-dimensional (2D) nearly free-electron gas. These Shockley-type surface states are dispersed as $\epsilon = \hbar^2 k^2 / 2m_{eff}$ (measured relative to the bottom of the surface-state band) and localized in narrow band gaps in the center of the first Brillouin zone of the (111)-projected bulk band structure. Thus they have extremely small Fermi wave vectors $k_f = \sqrt{2m_{eff}\epsilon_F}/\hbar$ and consequently the Friedel oscillations of the surface state have a significantly larger wavelength than those of the bulk states.

Recently, topological insulator (TI) has attracted tremendous experimental and theoretical studies [1, 2]. Unlike (111) surfaces of noble metals, a peculiar characteristic of TI is the presence of strong spin-orbit coupling (SOC), which results in a variety of unique properties. One intriguing fact is that the ideal TI surface is described at low energies by a 2D massless-Dirac wave equation with an additional locking between momentum and spin of surface electron. Because of the Dirac spectrum and SOC induced fermionic chirality, the impurity scattering effect in TIs is naturally expected to display novel behavior that should be absent from the conventional semiconductor or metal-surface 2D electron gases. Many experimental and theoretical efforts towards this issue have been paid. The anomalous Friedel oscillations in the vicinity of a single localized impurity [3–6], as well as the identification of the nature and the precise location of impurities on TI surface using STM [7–11], have been discussed. However, when impurities are located close to each other, multiple scattering effects should be important, such as the issue of the long-range interactions between the adsorbates mediated by the Dirac electrons of TI surface [12, 13]. In particular, since the quasiparticle's spin is strongly coupled to its momentum, quantum interference be-

tween different spin states during multiple scattering process could then display prominent phenomena such as electric conductance weak (anti-)localization [14] and Aharonov-Bohm effect [15] in STM signals.

In the presence of the time-reversal symmetry (TRS), the backscattering induced by nonmagnetic impurities is forbidden on the gapless TI surface because of a π Berry phase associated with the 2π adiabatic rotation of Dirac electron spin along the Fermi energy surface. However, considering the magnetic impurities on the gapless TI surface, one would like to observe the backscattering since the TRS is broken. Many efforts have been devoted to exploring this issue. For example, very recently, quasiparticle interference induced by a magnetic Co adatom on gapless Bi_2Se_3 surface has been found in STM experiments [16]. Furthermore, a magnetic field can be generated when the TI sample is deposited on a lithographically patterned ferromagnetic layer, which could also induce backscattering of massless Dirac electrons in TI [17].

Because of its importance both from basic point of interest and to TI-based chemical catalysis and electronics, in the present paper we address this issue by presenting a first attempt at the theoretical evaluation of the multiple scattering problem of the massless Dirac electrons on the TI surface in the presence of localized and identical magnetic impurities. Specially, we present the analytical expressions for multiple partial-wave scattering of massless Dirac electrons with magnetic impurities, based on which the asymptotic multiple scattering amplitude for random arraying magnetic impurities are obtained under the particular large distance approximations (the identical impurities are treated as a large scattering center). The differential and total cross sections (CSs), the inverse momentum relaxation time, and the Hall component of resistivity are discussed. We find that differing from the nonmagnetic scattering, for the magnetic impurity scattering, the CS is not convergent under s -wave approximation. Therefore, higher partial waves should be introduced. For the single magnetic impurity scattering, we show the fact that the backscattering becomes much stronger when increasing the effective magnetic moment M . By comparing the inverse momentum relaxation time with total CS, we can determine whether there exist more backscattering than forward scattering or not. Similar to CS, the inverse momentum relaxation time and Hall factor display oscillating behavior for multiple magnetic scattering centers due to interference.

II. MODEL AND THEORY

The eigenstates of the effective low-energy Hamiltonian of TI surface near the Dirac point [18]

$$H_0 = \hbar v_f (\boldsymbol{\sigma} \times \mathbf{k}) \cdot \hat{z} \quad (1)$$

are given by the spinors $\Psi_{0,\pm}(\mathbf{r}) = \frac{e^{i\mathbf{k} \cdot \mathbf{r}}}{\sqrt{2}} \begin{pmatrix} 1, \mp i e^{i\theta_{\mathbf{k}}} \end{pmatrix}^T$, where the upper/lower sign corresponds to the electron/hole part of the spectrum. Here, $v_f \sim 5 \times 10^5$ m/s is the Fermi velocity, $\boldsymbol{\sigma}$ are Pauli matrices, and \mathbf{k} is the in-plane wavevector. The impurity potential can be expressed as

$$V_i = \frac{1}{2} J_i \mathbf{S}_i \cdot \boldsymbol{\sigma} \Theta(a - r), \quad (2)$$

where $\mathbf{S}_i = S \mathbf{n}_i$ is the classical spin (with its orientation vector \mathbf{n}_i) of the i th magnetic impurity, J_i is the exchange coupling strengths, a is the radius of the scatterer, and $\Theta(r)$ is the Heaviside function. If the measurements are performed at a temperature higher than the Kondo temperature [19], the coupling between impurity spins will not exceed the critical value J_{cr} before a Kondo effect occurs. In this work we assume that the exchange coupling $J_i < J_{cr}$, so that the Ruderman-Kittel-Kasuya-Yosida interactions between impurity spins and Kondo screening of the impurity spin by the band electrons are neglected, and the impurity spin acts as a classical local magnetic moment under mean-field approximation [3, 4].

In order to obtain the analytical expressions of wavefunctions, we just consider the component of the classical spin along the normal line of TI surface, i.e., $V_i = M \sigma_z \Theta(a - r)$. The fact that a magnetic Co impurity with only perpendicular spin component on the TI surface does not open a gap has been experimentally observed [16]. To develop a scattering theory from localized, cylindrically-symmetric scatterers, it is convenient to resolve the problem in cylindrical coordinates. By considering the continuity of the wavefunction at the boundary of the magnetic scattering potential, one can immediately obtain the analytical expression of the scattered wave, written as

$$\Psi_{sc}(\mathbf{r}, \mathbf{k}, \pm) = s_0 G_{+0} T_0^- \Phi_{\pm}^{in} + \sum_{l=1}^{\infty} [s_l G_{+l} T_l^- + s_{-l} G_{-l} T_l^+] \Phi_{\pm}^{in}. \quad (3)$$

Here, Φ_{\pm}^{in} denotes the incident plane-wave centered about a single scatterer located at \mathbf{r}_n .

The cylindrically-symmetric Green's functions take the form

$$G_{+l} = \frac{i^l e^{il\theta_n}}{2} \begin{pmatrix} H_l^{(1)}(k\rho_n) & \pm H_l^{(1)}(k\rho_n) \\ \pm H_{l+1}^{(1)}(k\rho_n) e^{i\theta_n} & H_{l+1}^{(1)}(k\rho_n) e^{i\theta_n} \end{pmatrix}, \quad (4)$$

$$G_{-l} = \frac{i^l e^{-il\theta_n}}{2} \begin{pmatrix} H_l^{(1)}(k\rho_n) & \mp H_l^{(1)}(k\rho_n) \\ \mp H_{l-1}^{(1)}(k\rho_n) e^{i\theta_n} & H_{l-1}^{(1)}(k\rho_n) e^{i\theta_n} \end{pmatrix}, \quad (5)$$

for $|\epsilon| > M$, where upper and lower signs in the right side of these expressions denote the $\epsilon > 0$ and $\epsilon < 0$ parts of the spectrum, $k = \frac{\epsilon}{\hbar v_f}$, $\boldsymbol{\rho}_n = \mathbf{r} - \mathbf{r}_n$ and $e^{i\theta_n} = \frac{\boldsymbol{\rho}_n \cdot (\hat{x} + i\hat{y})}{\rho_n}$. For the energy regin of $|\epsilon| < M$, the Hankel functions $H_l^{(1)}(k\rho_n)$ in $G_{\pm l}$ should be replaced by the modified Bessel functions of first kind $I_l(k\rho_n)$. The scattering amplitude is expressed as

$$s_l = \frac{A_+ J_l(k'a) J_{l+1}(ka) - A_- J_l(ka) J_{l+1}(k'a)}{A_- H_l^{(1)}(ka) J_{l+1}(k'a) - A_+ H_{l+1}^{(1)}(ka) J_l(k'a)} \quad (6)$$

for $|\epsilon| > M$, where $A_{\pm} = \sqrt{|\epsilon \pm M|}$, $k' = \frac{\sqrt{|\epsilon^2 - M^2|}}{\hbar v_f}$, and J_l is the Bessel function of order l . Whereas s_l should also be replaced by

$$\tilde{s}_l = \frac{A_+ I_l(k'a) J_{l+1}(ka) + A_- J_l(ka) I_{l+1}(k'a)}{-A_- H_l^{(1)}(ka) I_{l+1}(k'a) - A_+ H_{l+1}^{(1)}(ka) I_l(k'a)} \quad (7)$$

for the case of for $|\epsilon| < M$. Note that s_l (\tilde{s}_l) satisfies the unitarity condition $\text{Re}[s_l] = -|s_l|^2$ ($\text{Re}[\tilde{s}_l] = -|\tilde{s}_l|^2$), and

$$\lim_{\epsilon \rightarrow M^+} s_l = \lim_{\epsilon \rightarrow M^-} \tilde{s}_l = -J_{l+1}(ka) / H_{l+1}(ka) \quad (8)$$

for all l . The l^{th} -partial-wave t -matrix is $T_l^{\pm} = \text{diag}(\hat{P}_l^{\pm}, \mp i \hat{P}_{l\mp 1}^{\pm})$ with $\hat{P}_l^{\pm} = \frac{e^{\pm il\theta}}{i^l k^l} (\partial_r \pm \frac{i}{r} \partial_{\theta})^l$. A detailed derivation is given in Appendix A.

It is easy to extend scattering theory of massless Dirac fermions to the realistic and reasonable case of multiple magnetic impurities, where the quantum interference effect in the propagation process of Dirac fermions on TI surface can be observed. This has not been discussed in previous studies, such as Ref. [17]. Taking into account all of partial waves, for N magnetic scatterers located at positions $\mathbf{r}_1, \mathbf{r}_2, \dots, \mathbf{r}_N$, the scattered wavefunction is given by

$$\Psi_{\text{sc}}(\mathbf{r}) = \mathbb{G}(\mathbf{r}) \mathbf{S} D^{-1} \vec{\phi}. \quad (9)$$

Here, $\mathbb{G}(\mathbf{r})$ (a $2 \times 2N$ ($2l_{\text{max}} + 1$) matrix) contains the propagation information from detector to impurities $G_{\pm l}(\mathbf{r}, \mathbf{r}_i)$. \mathbf{S} is a diagonal matrix with nonzero element $s_{\pm l}^{(n)}$. The \mathbf{G} matrix,

is constructed by $T_l^- [G_{\pm l'}(n, m)]$, describing the propagation between impurities. $\vec{\phi}$ can be written as a $2N(2l_{\max}+1) \times 1$ vector which imposes informations of incident waves (see details in Appendix B).

At this stage, we should point out that the above equations for multiple magnetic scattering of massless Dirac quasiparticles are similar to those for multiple nonmagnetic scattering of massive Dirac quasiparticles, but totally different from those for multiple nonmagnetic scattering of massless Dirac quasiparticles, since the expressions therein can be simplified as a more compact form due to $s'_{-(l+1)} = s'_l$.

The above theory enables to solve multiple magnetic scattering problems in gapless TI surfaces with higher partial waves, which could be important as distances between scatterers decrease or the scattering potential is strengthened. One simple application is to calculate the magnetic scattering CSs. To calculate the CSs, we have to take the approximations $H_l^{(1)}(z) \rightarrow \sqrt{\frac{2}{\pi z}} e^{i(z - \frac{l\pi}{2} - \frac{\pi}{4})}$, and $e^{il\theta_n} = \left[\frac{\rho_n \cdot (\hat{x} + i\hat{y})}{\rho_n} \right]^l \approx \left[\frac{\mathbf{r} \cdot (\hat{x} + i\hat{y})}{r} \right]^l = e^{il\varphi}$ for large distance. As a result,

$$\Psi_{\text{sc}}(\mathbf{r}) \rightarrow f(\mathbf{k}, \varphi) \frac{e^{ikr}}{\sqrt{2r}} \begin{pmatrix} 1 \\ \mp i e^{i\varphi} \end{pmatrix}, \quad (10)$$

where $f(\mathbf{k}, \varphi)$ is the scattering amplitude, from which we have the differential and total CSs as follows:

$$\frac{d\Lambda}{d\varphi} = |f(\mathbf{k}, \varphi)|^2, \quad (11)$$

$$\Lambda_{\text{tot}} = \int_0^{2\pi} d\varphi |f(\mathbf{k}, \varphi)|^2 = \sqrt{\frac{8\pi}{k}} \text{Im} [e^{-i\pi/4} f(\mathbf{k}, \varphi=0)]. \quad (12)$$

Here, we have used the two-dimensional optical theorem.

Besides, we could also obtain the transverse component of resistivity (or say the analog of Hall component in the case with magnetic field)

$$\Omega = \int_0^{2\pi} d\varphi |f(\mathbf{k}, \varphi)|^2 \sin \varphi, \quad (13)$$

and the inverse electron momentum relaxation time (the quantity proportional to the dissipative component of resistivity)

$$\Gamma_M = \int_0^{2\pi} d\varphi |f(\mathbf{k}, \varphi)|^2 (1 - \cos \varphi). \quad (14)$$

III. RESULTS AND DISCUSSIONS

In the following calculations, without losing the general properties, we shall just consider the incident wave $\Phi_+^{in} = \frac{e^{ikx}}{\sqrt{2}}(1, -i)^T$ propagating along the positive \hat{x} direction. In particular, for a single magnetic impurity scattering, we can obtain the scattering amplitude including all of the partial waves, which is written as

$$f(\mathbf{k}, \varphi) = \left\{ f_0(\varphi) + \sum_{l=1}^{\infty} [f_l(\varphi) + f_{-l}(\varphi)] \right\} e^{i(\mathbf{k} - k\hat{r}) \cdot \mathbf{r}'} \quad (15)$$

with $f_0(\varphi) = \sqrt{\frac{2}{i\pi k}} s_0$ and $f_{\pm l}(\varphi) = \sqrt{\frac{2}{i\pi k}} s_{\pm l} e^{\pm il\varphi}$. The differential and total CSs are given by

$$\frac{d\Lambda}{d\varphi} = \frac{2}{\pi k} \left| \left\{ s_0 + \sum_{l=1}^{\infty} [s_l e^{il\varphi} + s_{-l} e^{-il\varphi}] \right\} \right|^2, \quad (16)$$

$$\Lambda_{tot} = -\frac{4}{k} \left[\text{Re}(s_0) + \sum_{l=1}^{\infty} \text{Re}(s_l + s_{-l}) \right]. \quad (17)$$

This total CS equation is obtained from the optical theorem. It is clear that the s -wave is independent on the direction of scattered wave, therefore, we have to introduce higher partial waves, such as p - and d -waves, and so on. If one just considers the s -wave in calculations, differential CS may lead to an unreasonable result of $d\Lambda/d\varphi|_{\varphi=\pi} = 0$ (backscattering is forbidden) for some particular effective magnetic moment M . This is different from the nonmagnetic impurity scattering on TI surface [12] as well as on conventional 2DEG with weak Rashba SOC [20], where the s -wave approximation should be a reasonable choice.

The results of normalized differential CS as a function of energy ϵ for the massless Dirac electron scattered by a single magnetic impurity absorbed on TI surface with effective magnetic moment $M=60$ meV are shown in Fig. 1(a). In the calculations we take $l_{\max} = 2$, which works out convergent results. Different from the nonmagnetic impurity scattering case, the backscattering is obvious in the differential CS, i.e., $d\Lambda/d\varphi|_{\varphi=\pi} \neq 0$, in present case since the time-reversal symmetry is broken by magnetic impurity scattering. Furthermore, we find that for the weak effective magnetic moment M (such as the values chosen in this work $M \leq 100$ meV), the backscattering is greater than forward scattering. However, if the effective magnetic moment is large enough (for example, when $M \sim 500$ meV and $\epsilon = 450$ meV) we find the backscattering is weaker than the forward scattering (not shown here).

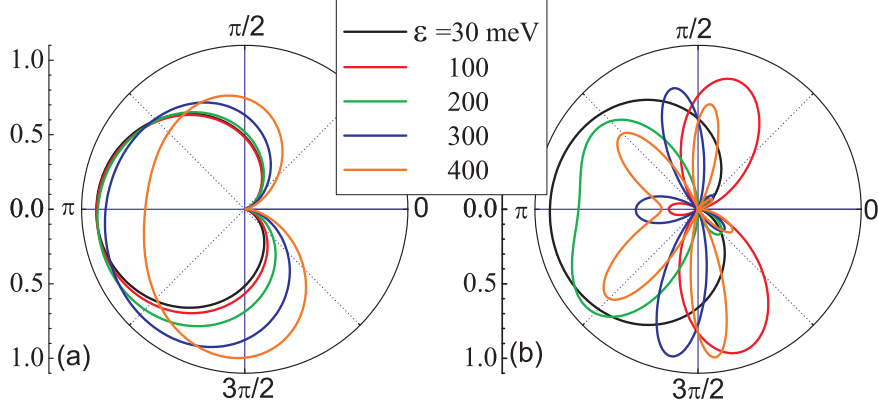


FIG. 1: (Color online) The normalized differential CSs $d\Lambda/d\phi$ for (a) a single and (b) two magnetic scatterers located at $\mathbf{r}_{1,2} = (\pm 3, 0)$ on TI surface with effective magnetic moment $M = 60$ meV. The radius of scatterer $a=1$ nm, and $l_{\max} = 2$ are chosen.

Two-impurity scattering provides a good test-bed to highlight the coexistence of various scattering phenomena, including transmission, reflection, interference, and resonance. The corresponding CS offers a measure of interaction events between the two impurity centers, and interference effects are useful in revealing actual electron density currents on TI surfaces. For instance, if two impurities are close to each other, the electronic wavefunctions will be scattered from both impurities, resulting in quantum interference. From the above theory, we can obtain the simple expression of scattering amplitude just containing the s -wave ($l_{\max} = 0$), which is given by

$$f_0^N(\mathbf{k}, \varphi) = \sum_{n,m=1}^N \frac{s_0 e^{i(\mathbf{k} \cdot \mathbf{r}_m - k\hat{\mathbf{r}} \cdot \mathbf{r}_n)}}{\sqrt{2i\pi k}} \times \left\{ [D^{-1}]_{(2n-1),(2m-1)} + [D^{-1}]_{2n,2m} \pm \left[[D^{-1}]_{2n,(2m-1)} + [D^{-1}]_{(2n-1),2m} \right] \right\}. \quad (18)$$

However, if higher partial waves ($l_{\max} \geq 1$) are taken into account, the scattering amplitude expression for N magnetic impurities becomes tedious and complex since D -matix becomes a lager one.

Typical numerical results of differential CSs for two magnetic impurities located at $\mathbf{r}_{1,2} = (\pm 3, 0)$ are presented in Fig. 1(b). We also note that the interference effect is related not only to the effective magnetic moment M but also to the configuration of impurities. For

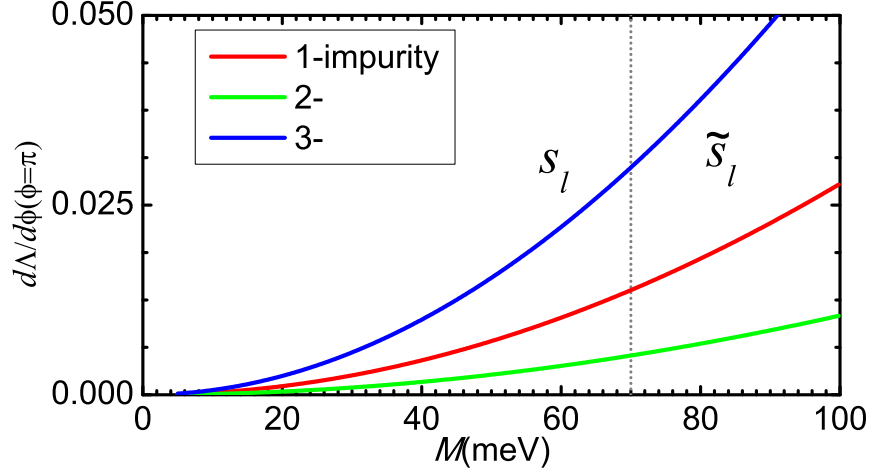


FIG. 2: (Color online) The magnetic moment M dependence of differential CS $d\Lambda/d\phi$ along the negative direction of x axis $\phi = \pi$ for one magnetic scatterer (red line), two scatterers (green line) located at $\mathbf{r}_{1,2} = (\pm 3, 0)$, and three scatterers (blue) located at $\mathbf{r}_1 = (-3, 0)$, $\mathbf{r}_2 = (3, -1)$, $\mathbf{r}_3 = (2, 4)$. The Fermi energy is chosen as $\epsilon = 70$ meV.

the present considered impurity locations $\mathbf{r}_{1,2}$, on one hand, we find from Fig. 1(b) that the backscattering is more prominent than the forward scattering. On the other hand, comparing with the nonmagnetic double-impurity scattering on gapless TI surface, the symmetry of differential CSs for two identical magnetic scatterers is reduced.

On one hand, independent on the impurity locations, with increasing the effective magnetic moment M , we find that the relative strength of backscattering becomes more and more remarkable since the differential CS along the negative \hat{x} direction $d\Lambda/d\phi|_{\phi=\pi}$ increases with M , see Fig. 2 with the Fermi energy $\epsilon = 70$ meV. On the other hand, comparing with the scattering from a single (red curve) magnetic impurity, two (green curve) or three (blue curve) impurities will weaken or strengthen the backscattering due to interference effect, which is dependent on the impurity configurations relative to the direction of incident wave. We must point out that in the calculations, we should use \tilde{s}_l for the energy region of $|\epsilon| < M$, while s_l for the energy region of $|\epsilon| > M$, which are denoted in Fig. 2.

Now let us turn to discuss the total CSs, which are exhibited in Fig. 3. As mentioned above, the s -wave approximation cannot give out convergent result, see the black curves in Fig. 3, whereas, when we introduce higher partial waves (such as $l_{\max} = 2$ chosen in our calculations), the total CSs becomes convergent ultimately. Differing from the nonmagnetic

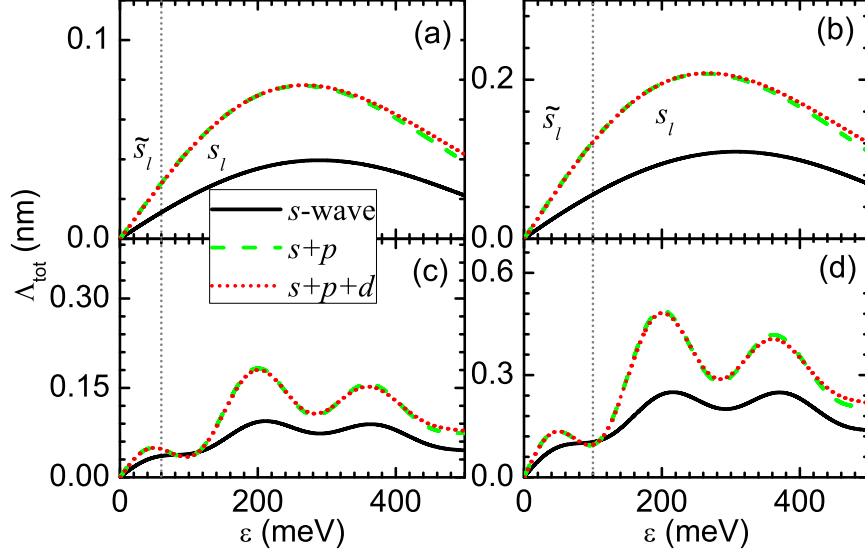


FIG. 3: (Color online) The total CS Λ_{tot} for a single (a-b) and two (c-d) magnetic impurities located at $\mathbf{r}_{1,2} = (\pm 3, 0)$. The effective magnetic moment is chosen as $M = 60$ meV in (a) and (c), while $M = 100$ meV in (b) and (d), respectively.

impurity scattering, although the higher partial waves can induce remarkable corrections, we have not found additional resonant peaks in total CSs due to higher partial waves. Moreover, it is obvious that interference between double impurities brings about oscillations in total CSs (see Figs. 3(c) and 3(d)), which cannot be observed in the case of nonmagnetic impurity scattering [12]. From numerical calculations, we find on one hand that, the optical theorem is correct and should characterize the general multiple-scattering processes, since the results obtained by the numerical integration of the first equality in Eq. (12) are in good agreement with that obtained from the second equality; On the other hand, the curves of total CSs are smooth at the energy of $\epsilon = M$, which indicates that the limiting function of s_l and \tilde{s}_l , i.e., Eq. (8) is reasonable. Besides, for the much strong effective magnetic impurity scattering, with increasing the Fermi energy we find that the total CS for single- (double-) impurity is convergent to 4 nm (8 nm). This is also different from the nonmagnetic impurity scattering, where the total CSs converge to zero with increasing the energy of Dirac electrons [12].

In spite of the differential and total CSs, we also calculated the transverse component of resistivity Ω , which is analogous to Hall component in the case with external magnetic field. The typical results of Ω as a function of ϵ for single- and double-impurity with different

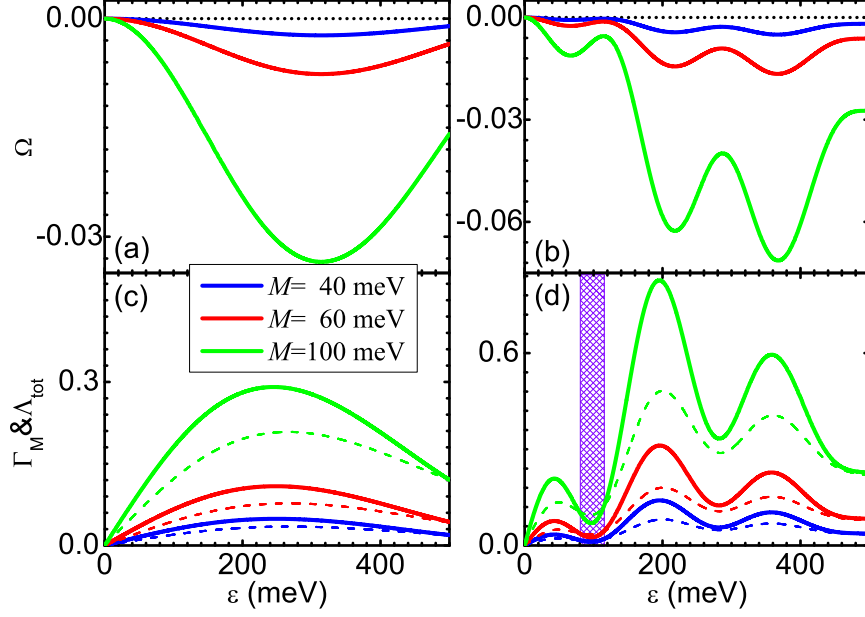


FIG. 4: (Color online) Hall component of resistivity Ω for a single (a) and two (b) magnetic impurities on TI surface; Inverse momentum relation time Γ_M (thick solid curves) and total CS Λ_{tot} (thin dashed curved) for a single (c) and two (d) magnetic impurities as functions of energy ϵ .

M are listed in Figs. 4(a) and 4(b), respectively. We find that the Hall component of the resistivity Ω always keeps its sign as negative (i.e., $\Omega < 0$), which is independent on the impurity locations. In the numerical calculations, we take $l_{\max} \geq 2$ which results in a convergent result, however, taking into account higher partial waves, it is difficult to be obtained analytically from Eqs. (13) and (15) since the expression for integral result is tedious and complex. Therefore, the low-energy Dirac electrons are deflected to one side of TI sample due to magnetic impurity scattering. This fact may be helpful for tuning the Hall voltage of sample. Interestingly, we note that this type of Hall component also occurs in the nonmagnetic impurity scattering on gapless TI surface. We now switch gears and consider the case of double magnetic impurities on TI surface again. Different from the single case, Ω exhibits oscillating behavior due to the interference during the multiple impurities scattering processes, as shown in Fig. 4(b).

Before ending this paper, we would like to discuss another important quantity, the inverse electron momentum relaxation time Γ_M , which is proportional to the dissipative component of resistivity. The numerical results are plotted in Figs. 4(c) and 4(d) for single- and double-

impurity cases, respectively. The behavior of Γ_M (thick solid curves) is qualitatively similar to the one for the total CSs Λ_{tot} (thin dashed curves), and the interference effect is also clear in the Γ_M induced by double-impurity, see Fig. 4(d). The inverse electron momentum relaxation time Γ_M is a fairly sensitive quantity that determines whether the charge carrier is attracted to an impurity or is repelled from it. It is also useful for determining whether the backscattering is greater than the forward scattering by comparing it with the total CSs (note that both Λ_{tot} and Γ_M have the dimension of an length in two dimensional scattering). If $\Lambda_{tot} < \Gamma_M$ ($\Lambda_{tot} > \Gamma_M$), there is more (less) backscattering than forward scattering. Taking $M = 60$ meV as an example, we find $\Lambda_{tot} < \Gamma_M$, as revealed by the red curves in Fig. 4(c), which indicates that the backscattering is greater than the forward scattering in the low-energy region. This fact is consistent with the behavior of differential CSs shown in Fig. 1(a). Particularly, by observing the green curves in Fig. 4(d) of energy region of 80~120 meV (the shadow region), one can find $\Lambda_{tot} > \Gamma_M$. This suggests that due to the interference the backscattering is weaker than forward scattering in this energy region for the present double magnetic impurity locations, which is also consistent with the analysis of differential CSs. Consequently, we believe that our results shown here are reasonable, and we hope our findings could be detected in the future experiments.

IV. CONCLUSIONS

In summary, we have proposed a general low-energy multiple-scattering partial-wave theory for quasiparticles on the gapless topological insulator (TI) surfaces in the presence of magnetic impurities. Based on this theory, one can solve the scattering problems of N magnetic impurities. As an application, we have calculated the CSs, the inverse momentum relaxation time, and the transverse resistivity component for a single and two circular magnetic scattering. We have found that the usual s -wave approximation is not sufficient, while higher partial waves must be introduced to obtain convergent results. On the gapless TI surfaces, differing from the single nonmagnetic impurity case, the backscattering occurs and becomes much stronger with increasing the effective magnetic moment M . Interference effects are obvious in CSs from quasiparticle scattering off two magnetic scattering centers, and oscillating behaviors are introduced in Λ_{tot} associated with higher-order partial-waves. A non-zero perpendicular resistivity component has also been shown. Similar to the total

CS, the inverse momentum relaxation time and the transverse resistivity component exhibit oscillations for multiple magnetic scattering centers due to interference. Furthermore, our theory could be extended to spin-polarized case. It could also be applied to simulate the electron flow (charge current and spin current) through a quantum point contact on a TI surface by monitoring the changes in conductance through the quantum point contact as a moveable STM tip is scanned above the surface of TI.

Acknowledgments

This work was supported by NSFC under Grants No. 90921003, No. 60776063, and No. 60821061, and by the National Basic Research Program of China (973 Program) under Grants No. 2009CB929103 and No. G2009CB929300.

APPENDIX A: DERIVATION DETAILS OF SCATTERED WAVEFUNCTION

Starting from the model considered in the main text, one can find the spinor spherical wavefunctions inside the magnetic scattering potential ($r < a$) as follows:

$$\zeta_l^{(1,2)}(\mathbf{r}, k', \pm) = \frac{we^{i\theta}}{\sqrt{2|\epsilon|k'}} \begin{pmatrix} \sqrt{|\epsilon + M|} H_l^{(1,2)}(k'r) \\ \pm \sqrt{|\epsilon - M|} H_{l+1}^{(1,2)}(k'r) e^{i\theta} \end{pmatrix}, \quad (|\epsilon| > M), \quad (\text{A1})$$

$$\tilde{\zeta}_l(\mathbf{r}, k', \pm) = \frac{we^{i\theta}}{\sqrt{2|\epsilon|k'}} \begin{pmatrix} \sqrt{|\epsilon + M|} I_l(k'r) \\ \mp \sqrt{|\epsilon - M|} I_{l+1}(k'r) e^{i\theta} \end{pmatrix}, \quad (|\epsilon| < M), \quad (\text{A2})$$

where $k' = \frac{\sqrt{|\epsilon^2 - M^2|}}{\hbar v_f}$ and $w = e^{i\phi}$ is an overall phase meaning of the nonrelativistic wavefunction in the rest frame of $\epsilon = M$. Here, $H_l^{(1,2)}(z)$ and $I_l(z)$ are l^{th} -order Hankel functions and modified Bessel functions of first kind, respectively. We would like to point out that since the wavefunctions should be zero at $r = 0$, we have neglected the modified Bessel functions of second kind $K_l(z)$ for $|\epsilon| < M$, which are emanative in the limit of $z \rightarrow 0$. Whereas, the wavefunctions outside the magnetic potential ($r > a$) can be expressed as

$$\chi_{l,\pm}^{(1,2)}(\mathbf{r}) = \frac{1}{\sqrt{2k}} \begin{pmatrix} H_l^{(1,2)}(kr) e^{il\theta} \\ \pm H_{l+1}^{(1,2)}(kr) e^{i(l+1)\theta} \end{pmatrix}, \quad (\text{A3})$$

with $k = \frac{\epsilon}{\hbar v_f}$. $\chi^{(1)}$ ($\chi^{(2)}$) denotes the outgoing (incoming) cylindrical wave about $\mathbf{r}=0$. The incident plane-wave centered about a single scatterer located at \mathbf{r}_n is given by

$$\Phi_{\pm}^{in}(\mathbf{r}) = \sum_{l=-\infty}^{\infty} \frac{\sqrt{k} e^{i\mathbf{k} \cdot \mathbf{r}_n} e^{il(\theta_n - \theta_{\mathbf{k}})}}{2} i^l \left(\chi_{l,\pm}^{(1)}(\rho_n) + \chi_{l,\pm}^{(2)}(\rho_n) \right), \quad (\text{A4})$$

where $\rho_n = \mathbf{r} - \mathbf{r}_n$ and $e^{i\theta_n} = \frac{\rho_n \cdot (\hat{x} + i\hat{y})}{\rho_n}$. Remember that $\theta_{\mathbf{k}}$ is the angle defining the direction of the wave vector, and θ_n is related to the direction of $\mathbf{r} - \mathbf{r}_n$ in this equation. Then, the fully scattered wave function in the region $\rho_n > a$ can be written as explicitly

$$\begin{aligned} \Psi_I(\mathbf{r}, \mathbf{k}, \pm) &= \Phi_{\pm}^{in}(\mathbf{r}) + \Psi_{sc}(\mathbf{r}, \mathbf{k}, \pm) \\ &= \sqrt{k} e^{i\mathbf{k} \cdot \mathbf{r}_n} \sum_{l=-\infty}^{\infty} i^l \left[\frac{1}{2} e^{2i\delta_l} \chi_l^{(1)}(\rho_n, \mathbf{k}, \pm) + \frac{1}{2} \chi_l^{(2)}(\rho_n, \mathbf{k}, \pm) \right] e^{il(\theta_n - \theta_{\mathbf{k}})}, \end{aligned} \quad (\text{A5})$$

where δ_l are phase shifts of the outgoing cylindrical partial waves, $\chi_l^{(1)}(\rho_n, \mathbf{k}, \pm)$. In the region of $\rho_n \leq a$, the fully scattered wave function is given by

$$\Psi_{II}(\mathbf{r}, \mathbf{k}', \pm) = \begin{cases} \sqrt{k'} e^{i\mathbf{k}' \cdot \mathbf{r}_n} \sum_{l=-\infty}^{\infty} i^l d_l \left[\frac{1}{2} \zeta_l^{(1)}(\rho_n, \mathbf{k}', \pm) - \frac{1}{2} \zeta_l^{(2)}(\rho_n, \mathbf{k}', \pm) \right] e^{il(\theta_n - \theta_{\mathbf{k}})}, & (|\epsilon| > M) \\ \sqrt{k'} e^{i\mathbf{k}' \cdot \mathbf{r}_n} \sum_{l=-\infty}^{\infty} i^l \tilde{d}_l \tilde{\zeta}_l(\mathbf{r}, \mathbf{k}', \pm) e^{il(\theta_n - \theta_{\mathbf{k}})}, & (|\epsilon| < M) \end{cases}. \quad (\text{A6})$$

By the continuity of the wavefunction at $\rho_n = a$, $\Psi_I(\mathbf{a}, \mathbf{k}, \pm) = \Psi_{II}(\mathbf{a}, \mathbf{k}', \pm)$, we can obtain the scattered wavefunction Eq. (3), and the scattering amplitude s_l and \tilde{s}_l shown in Eqs. (6) and (7) in main text. It is clear that the scattered wavefunctions shown in Eq. (3) are different from those for nonmagnetic impurity scattering on gapless TI surface, where

$$\Psi_{sc}(\mathbf{r}) = \sum_{l=0}^{\infty} \frac{4i\hbar v_f s'_l}{k} G_l(\mathbf{r}, \mathbf{r}_n, \epsilon) T'_l [\Phi_{\pm}^{in}] \quad (\text{A7})$$

with

$$G_l \propto \begin{pmatrix} H_l^{(1)} e^{il\theta_n} & \mp H_{l+1}^{(1)} e^{-i(l+1)\theta_n} \\ \pm H_{l+1}^{(1)} e^{i(l+1)\theta_n} & H_l^{(1)} e^{-il\theta_n} \end{pmatrix}, \quad (\text{A8})$$

$T'_l = \text{diag}(\hat{P}_l^-, \hat{P}_l^+)$, and

$$s'_l = \frac{J_l(\kappa' a) J_{l+1}(ka) - J_l(ka) J_{l+1}(\kappa' a)}{H_l^{(1)}(ka) J_{l+1}(\kappa' a) - H_{l+1}^{(1)}(ka) J_l(\kappa' a)}. \quad (\text{A9})$$

Here $\kappa' = \frac{\epsilon - V_0}{\hbar v_f}$, and V_0 is the scalar potential.

APPENDIX B: DETAILS OF THE EXPEDITION FOR MULTIPLE SCATTERED WAVE

In order to understand the extending operation, we would like to start from the s -wave scattering for two identical magnetic impurities. The total wavefunction can be written as

$$\Psi(\mathbf{r}) = \Phi(\mathbf{r}) + \sum_{n=1}^2 s_0^{(n)} G_{+0}(\mathbf{r}, \mathbf{r}_n, \epsilon) T_0^- [\Psi_n(\mathbf{r}_n, \mathbf{k}, \pm)], \quad (\text{B1})$$

where

$$\Psi_n(\mathbf{r}) = \Phi(\mathbf{r}) + \sum_{m \neq n}^2 s_0^{(m)} G_{+0}(\mathbf{r}, \mathbf{r}_m, \epsilon) T_0^- [\Psi_m(\mathbf{r}_m, \mathbf{k}, \pm)]. \quad (\text{B2})$$

Equation (B1) indicates that if the value of $\Psi(\mathbf{r})$ and its derivatives due to the $\hat{P}_{0,1}^\pm$ dependence of T_0^\pm at each scatterer is known, the entire wavefunction $\Psi(\mathbf{r})$ is completely determined. We can calculate the derivatives of Ψ_1 at \mathbf{r}_1 and Ψ_2 at \mathbf{r}_2 and combine the result into a matrix equation, which are given by

$$\begin{pmatrix} T_0^- [\Psi_1(\mathbf{r}_1)] \\ T_0^- [\Psi_2(\mathbf{r}_2)] \end{pmatrix} = D^{-1} \begin{pmatrix} T_0^- [\Phi(\mathbf{r}_1)] \\ T_0^- [\Phi(\mathbf{r}_2)] \end{pmatrix}, \quad (\text{B3})$$

where

$$D = \mathbf{1}_{4 \times 4} - \mathbf{G}_{4 \times 4} \mathbf{S}_{4 \times 4}, \quad (\text{B4})$$

with

$$\mathbf{G} = \begin{pmatrix} \mathbf{0} & T_0^- [G_{+0}(\mathbf{r}_1, \mathbf{r}_2, \epsilon)] \\ T_0^- [G_{+0}(\mathbf{r}_2, \mathbf{r}_1, \epsilon)] & \mathbf{0} \end{pmatrix}, \quad (\text{B5})$$

$$\mathbf{S} = \begin{pmatrix} s_0^{(1)} & 0 \\ 0 & s_0^{(2)} \end{pmatrix} \otimes \mathbf{1}_{2 \times 2}. \quad (\text{B6})$$

Finally, the total wavefunction is written as

$$\Psi(\mathbf{r}) = \Phi_\pm^{in} + \mathbb{G}(\mathbf{r}) \mathbf{S} D^{-1} \begin{pmatrix} T_0^- [\Phi(\mathbf{r}_1)] \\ T_0^- [\Phi(\mathbf{r}_2)] \end{pmatrix} \quad (\text{B7})$$

with

$$\mathbb{G}(\mathbf{r}) = \begin{pmatrix} G_{+0}(\mathbf{r}, \mathbf{r}_1), & G_{+0}(\mathbf{r}, \mathbf{r}_2) \end{pmatrix}. \quad (\text{B8})$$

Taking into account $l_{\max} \geq 1$ partial waves, for N magnetic scatterers located at positions $\mathbf{r}_1, \mathbf{r}_2, \dots, \mathbf{r}_N$, the scattered wavefunction is given by Eq. (9) in main text. For numerical

calculations, we have to align the matrix elements reasonably, thereby, we define symbols $\mu_0 = 2(n-1)(2l_{\max}+1)+1$, $\lambda_0 = \mu_0 + 1$, $\alpha_0 = 2(n-1)(2l_{\max}+1)+4l-1$, $\gamma_0 = \alpha_0 + 1$, $\tau_0 = 2(n-1)(2l_{\max}+1)+4l+1$, $\eta_0 = \tau_0 + 1$, $\nu_0 = 2(m-1)(2l_{\max}+1)+1$, $\beta_0 = \nu_0 + 1$, $\alpha = 2(m-1)(2l_{\max}+1)+4l'-1$, $\gamma = \alpha + 1$, $\nu = 2(m-1)(2l_{\max}+1)+4l'+1$, and $\beta = \nu + 1$. Following this way $\mathbb{G}(\mathbf{r})$ (a $2 \times 2N(2l_{\max}+1)$ matrix) is aligned as

$$\mathbb{G}(\mathbf{r}) = \left(\tilde{G}(\mathbf{r}, \mathbf{r}_1), \tilde{G}(\mathbf{r}, \mathbf{r}_2), \dots, \tilde{G}(\mathbf{r}, \mathbf{r}_N) \right) \quad (\text{B9})$$

with $\tilde{G}(\mathbf{r}, \mathbf{r}_i) = [G_{+0}, G_{+1}, G_{-1}, \dots, G_{+l_{\max}}, G_{-l_{\max}}]$. Explicitly, for $l = 0$, we align

$$\begin{pmatrix} \mathbb{G}(\mathbf{r})_{1,\mu_0} & \mathbb{G}(\mathbf{r})_{1,\lambda_0} \\ \mathbb{G}(\mathbf{r})_{2,\mu_0} & \mathbb{G}(\mathbf{r})_{2,\lambda_0} \end{pmatrix} = G_{+0}(\mathbf{r}, \mathbf{r}_n), \quad (\text{B10})$$

and for $l \geq 1$,

$$\begin{pmatrix} \mathbb{G}(\mathbf{r})_{1,\alpha_0} & \mathbb{G}(\mathbf{r})_{1,\gamma_0} \\ \mathbb{G}(\mathbf{r})_{2,\alpha_0} & \mathbb{G}(\mathbf{r})_{2,\gamma_0} \end{pmatrix} = G_{+l}(\mathbf{r}, \mathbf{r}_n), \quad (\text{B11})$$

$$\begin{pmatrix} \mathbb{G}(\mathbf{r})_{1,\tau_0} & \mathbb{G}(\mathbf{r})_{1,\eta_0} \\ \mathbb{G}(\mathbf{r})_{2,\tau_0} & \mathbb{G}(\mathbf{r})_{2,\eta_0} \end{pmatrix} = G_{-l}(\mathbf{r}, \mathbf{r}_n). \quad (\text{B12})$$

The S matrix is diagonal,

$$\mathbf{S} = \text{diag} \left(s_{\pm l}^{(n)} \right)_{2N(2l_{\max}+1) \times 2N(2l_{\max}+1)}, \quad (\text{B13})$$

with $\mathbf{S}_{\mu_0,\mu_0} = \mathbf{S}_{\lambda_0,\lambda_0} = s_{+0}^{(n)}$, $\mathbf{S}_{\alpha_0,\alpha_0} = \mathbf{S}_{\gamma_0,\gamma_0} = s_{+l}^{(n)}$, $\mathbf{S}_{\tau_0,\tau_0} = \mathbf{S}_{\eta_0,\eta_0} = s_{-l}^{(n)}$. Then we construct the \mathbf{G} matrix, which is written as

$$\mathbf{G} = \begin{pmatrix} 0 & G(1,2) & \dots & G(1,N) \\ G(2,1) & 0 & \dots & G(2,N) \\ \vdots & \vdots & \ddots & \vdots \\ G(N,1) & G(N,2) & \dots & 0 \end{pmatrix}, \quad (\text{B14})$$

where $G(n, m)$ is a $2(2l_{\max} + 1) \times 2(2l_{\max} + 1)$ matrix, which are constructed by $T_l^- [G_{\pm l'}(n, m)]$. Explicitly, one would align the \mathbf{G} matrix by the following way

$$\begin{pmatrix} \mathbf{G}(\mu_0, \nu_0) & \mathbf{G}(\mu_0, \beta_0) \\ \mathbf{G}(\lambda_0, \nu_0) & \mathbf{G}(\lambda_0, \beta_0) \end{pmatrix} = T_0^- [G_{+0}(n, m)], \quad (\text{B15})$$

$$\begin{pmatrix} \mathbf{G}(\mu_0, \alpha) & \mathbf{G}(\mu_0, \gamma) \\ \mathbf{G}(\lambda_0, \alpha) & \mathbf{G}(\lambda_0, \gamma) \end{pmatrix} = T_0^- [G_{+l'}(n, m)], \quad (\text{B16})$$

$$\begin{pmatrix} \mathbf{G}(\mu_0, \nu) & \mathbf{G}(\mu_0, \beta) \\ \mathbf{G}(\lambda_0, \nu) & \mathbf{G}(\lambda_0, \beta) \end{pmatrix} = T_0^- [G_{-l'}(n, m)], \quad (\text{B17})$$

for $l = 0$ and $n \neq m$, and

$$\begin{pmatrix} \mathbf{G}(\alpha_0, \nu_0) & \mathbf{G}(\alpha_0, \beta_0) \\ \mathbf{G}(\gamma_0, \nu_0) & \mathbf{G}(\gamma_0, \beta_0) \end{pmatrix} = T_l^- [G_{+0}(n, m)], \quad (\text{B18})$$

$$\begin{pmatrix} \mathbf{G}(\alpha_0, \alpha) & \mathbf{G}(\alpha_0, \gamma) \\ \mathbf{G}(\gamma_0, \alpha) & \mathbf{G}(\gamma_0, \gamma) \end{pmatrix} = T_l^- [G_{+l'}(n, m)], \quad (\text{B19})$$

$$\begin{pmatrix} \mathbf{G}(\alpha_0, \nu) & \mathbf{G}(\alpha_0, \beta) \\ \mathbf{G}(\gamma_0, \nu) & \mathbf{G}(\gamma_0, \beta) \end{pmatrix} = T_l^- [G_{-l'}(n, m)], \quad (\text{B20})$$

$$\begin{pmatrix} \mathbf{G}(\tau_0, \nu_0) & \mathbf{G}(\tau_0, \beta_0) \\ \mathbf{G}(\eta_0, \nu_0) & \mathbf{G}(\eta_0, \beta_0) \end{pmatrix} = T_l^+ [G_{+0}(n, m)], \quad (\text{B21})$$

$$\begin{pmatrix} \mathbf{G}(\tau_0, \alpha) & \mathbf{G}(\tau_0, \gamma) \\ \mathbf{G}(\eta_0, \alpha) & \mathbf{G}(\eta_0, \gamma) \end{pmatrix} = T_l^+ [G_{+l'}(n, m)], \quad (\text{B22})$$

$$\begin{pmatrix} \mathbf{G}(\tau_0, \nu) & \mathbf{G}(\tau_0, \beta) \\ \mathbf{G}(\eta_0, \nu) & \mathbf{G}(\eta_0, \beta) \end{pmatrix} = T_l^+ [G_{-l'}^k(n, m)], \quad (\text{B23})$$

for $l \neq 0$ and $n \neq m$, while $\mathbf{G}(n, n) = 0$ for $n = m$. $\vec{\phi}$ can be written as a $2N(2l_{\max} + 1) \times 1$ vector,

$$\vec{\phi} = \left(\phi_1, \phi_2, \dots, \phi_N \right)^T, \quad (\text{B24})$$

where $\phi_i = \left[T_0^- [\Phi(\mathbf{r}_i)], T_1^- [\Phi(\mathbf{r}_i)], T_1^+ [\Phi(\mathbf{r}_i)], \dots, T_{l_{\max}}^- [\Phi(\mathbf{r}_i)], T_{l_{\max}}^+ [\Phi(\mathbf{r}_i)] \right]^T$.

Explicitly, for $l' = 0$,

$$\vec{\phi}_{\nu_0} = P_0^- \left[e^{i\mathbf{k} \cdot \mathbf{r}_n} / \sqrt{2} \right], \vec{\phi}_{\beta_0} = iP_1^- \left[\mp i e^{i\theta_k} e^{i\mathbf{k} \cdot \mathbf{r}_n} / \sqrt{2} \right]. \quad (\text{B25})$$

For $l' > 0$,

$$\vec{\phi}_\alpha = P_{l'}^- \left[e^{i\mathbf{k}\cdot\mathbf{r}_n} / \sqrt{2} \right], \vec{\phi}_\gamma = iP_{l'+1}^- \left[\mp i e^{i\theta_k} e^{i\mathbf{k}\cdot\mathbf{r}_n} / \sqrt{2} \right], \quad (\text{B26})$$

$$\vec{\phi}_\nu = P_{l'}^+ \left[e^{i\mathbf{k}\cdot\mathbf{r}_n} / \sqrt{2} \right], \vec{\phi}_\beta = iP_{l'+1}^+ \left[\pm i e^{i\theta_k} e^{i\mathbf{k}\cdot\mathbf{r}_n} / \sqrt{2} \right]. \quad (\text{B27})$$

-
- [1] M. Z. Hasan and C. L. Kane, Rev. Mod. Phys. **82**, 3045 (2010).
 - [2] X.-L. Qi and S.-C. Zhang, Rev. Mod. Phys. **83**, 1057 (2011).
 - [3] Q. Liu, C.-X. Liu, C. Xu, X.-L. Qi, and S.-C. Zhang, Phys. Rev. Lett. **102**, 156603 (2009).
 - [4] R. R. Biswas and A. V. Balatsky, Phys. Rev. B **81**, 233405(R) (2010).
 - [5] R. R. Biswas and A. V. Balatsky, Phys. Rev. B **83**, 075439 (2011).
 - [6] A. M. Black-Schaffer, and A. V. Balatsky, Phys. Rev. B **85**, 121103(R) (2012).
 - [7] T. Zhang, P. Cheng, X. Chen, J.-F. Jia, X. Ma, K. He, L. Wang, H. Zhang, X. Dai, Z. Fang, X. Xie, and Q.-K. Xue, Phys. Rev. Lett. **103**, 266803 (2009).
 - [8] P. Roushan, J. Seo, C. V. Parker, Y. S. Hor, D. Hsieh, D. Qian, A. Richardella, M. Z. Hasan, R. J. Cava, A. Yazdani, Nature **460**, 1106 (2009).
 - [9] J. Wang, W. Li, P. Cheng, C. Song, T. Zhang, P. Deng, X. Chen, X. Ma, K. He, J.-F. Jia, Q.-K. Xue, and B.-F. Zhu, Phys. Rev. B **84**, 2135447 (2011).
 - [10] Z. Alpichshev, J. G. Analytis, J.-H. Chu, I. R. Fisher, Y. L. Chen, Z. X. Shen, A. Fang, and A. Kapitulnik, Phys. Rev. Lett. **104**, 016401 (2011).
 - [11] Z. Alpichshev, R. R. Biswas, A. V. Balatsky, J. G. Analytis, J.-H. Chu, I. R. Fisher, A. Kapitulnik, Phys. Rev. Lett. **108**, 206402 (2012).
 - [12] Z.-G. Fu, P. Zhang, Z. Wang, and S.-S. Li, Appl. Phys. Lett. **99**, 232109 (2011).
 - [13] Z.-G. Fu, P. Zhang, Z. Wang, and S.-S. Li, Phys. Rev. B, **84**, 235438 (2011).
 - [14] H.-T. He, G. Wang, T. Zhang, I.-K. Sou, G. K. L Wong, J.-N. Wang, H.-Z. Lu, S.-Q. Shen, and F.-C. Zhang, Phys. Rev. Lett. **106**, 166805 (2011).
 - [15] Z.-G. Fu, P. Zhang, and S.-S. Li, Appl. Phys. Lett. **99**, 243110 (2011).
 - [16] M. Ye, S. V. Eremeev, K. Kuroda, E. E. Krasovskii, E. V. Chulkov, Y. Takeda, Y. Saitoh, K. Okamoto, S. Y. Zhu, K. Miyamoto, M. Arita, M. Nakatake, T. Okuda, Y. Ueda, K. Shimada, H. Namatame, M. Taniguchi, A. Kimura, Phys. Rev. B **85**, 205317 (2012).
 - [17] A. Zazunov, A. Kundu, A. Hütten, and R. Egger, Phys. Rev. B **82**, 155431 (2010).

- [18] H.-J. Zhang, C.-X. Liu, X.-L. Qi, X. Dai, Z. Fang, and S.-C. Zhang, *Nature Phys.* **5**, 438 (2009).
- [19] J. J. Cha, J. R. Williams, D. Kong, S. Meister, H. Peng, A. J. Bestwick, P. Gallagher, D. Goldhaber-Gordon, and Y. Cui, *Nano Lett.* **10**, 1076, (2010).
- [20] J. D. Walls, J. Huang, R. M. Westervelt, and E. J. Heller, *Phys. Rev. B* **73**, 035325 (2006).